ACS SENSORS

pubs.acs.org/acssensors

Article

Metal Cluster-Based Electrochemical Biosensing System for Detecting Epithelial-to-Mesenchymal Transition

Ying Han, Cuicui Qiu, Jiaojiao Li, Fuping Gao, Qing Yuan, Yuhua Tang, Wenchao Niu, Xiayan Wang, Xueyun Gao, and Liang Gao*

Cite This: *ACS Sens.* 2021, 6, 2290–2298

Read Online

ACCESS | Metrics & More | Article Recommendations | Supporting Information

ABSTRACT: N-cadherin serves as an important oncobiomarker of epithelial-to-mesenchymal transition (EMT) progression, which identifies invasion and metastasis of malignant tumor cells. Although many efforts have been devoted to quantitative detection of N-cadherin, efforts to analyzing the protein of interest at intact cellular levels are scarce. Herein, a metal cluster-based electrochemical biosensing system is developed to determine the expressing levels of N-cadherin during the EMT process of tumor cells. To be specific, a peptide with a unique sequence and function is designed as a reductant and an anchor to synthesize metal clusters in a precise manner. Consequently, peptide-modified metal clusters possess N-cadherin-targeting, photoluminescence, and electrocatalytic properties. Especially, the redox-active metal clusters function as both an electron-transfer mediator and an electronic conductor for enhanced electrochemical sensing. These favorable features enable them as a rapid, sensitive, and reliable whole-cell biosensor, which integrates the fluorescence and electrochemical signals. This cytosensor can accurately quantify the expression levels of N-cadherin on at least 5000 tumor cells. Further, the current signals of model cancer cells gradually increase with EMT progression, indicating tumor cell-type evolution. Our study represents the advanced bioprobe and analytical methods for accurate quantitation of a biomarker to identify tumor progression.

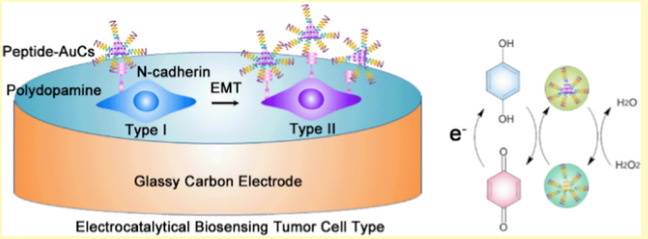

KEYWORDS: *metal clusters, epithelial-to-mesenchymal transition, N-cadherin, in situ electrochemical analysis, biosensor*

Numerous efforts have been devoted to the development of advantageous methods for early detection and quantitative measurement of cancer biomarkers to obtain information correlated to tumorigenesis.[1] Epithelial-to-mesenchymal transition (EMT) is a typical feature during the migration and invasion of epithelial-derived malignant tumor cells.[2] At the molecular level, the main characteristics are the downregulated expression of epithelial phenotypic markers such as E-cadherin and the upregulated expression of interstitial phenotypic markers such as N-cadherin.[3,4] In particular, N-cadherin is a class of calcium-dependent transmembrane glycoproteins that mediate homotypic and heterotypic cell−cell adhesion.[5] In recent years, evidence has shown that overexpressed N-cadherin endows tumor cells with enhanced migratory and invasive capacities.[6] Thus, N-cadherin in EMT progression is utilized as a diagnostic biomarker of tumor invasion and metastasis. So far, many bioanalytical platforms have been developed for detecting oncobiomarkers, including enzyme-linked immunosorbent assay (ELISA),[7] electrophoresis,[8] colorimetric assays,[9] fluorescence imaging,[10] mass spectrometry,[11] and biochip methods.[12] However, these techniques heavily relied on the analysis of oncobiomarkers after cells or tissue lysis, and the loss of biomarkers and the interference of multiple biomarkers during the analysis is inevitable. Moreover, these techniques normally require expensive equipment, professional operators, and long turnaround times. We envision establishing an accurate, rapid, sensitive, simple, and low-cost method for in situ quantitative analysis of tumor biomarkers without cell lysis.

Electrochemical strategies such as voltammetric, amperometry, and impedimetric techniques have been increasingly used for the detection of tumor biomarkers due to the advantages of good portability, high sensitivity, low cost, and fast response.[13−16] The critical point is developing specific electrode materials with high activity and sensitivity as an advanced biosensor to detect specific tumor biomarkers with low concentration. Metal clusters possess many physiochemical advantages, such as accurate composition and size-specific electrochemical, optical, and catalytic activities, ascribed to unique quantum confinement effects and geometric structures.[17] Compared to bulk electrocatalysts and traditional

Received: February 17, 2021
Accepted: May 13, 2021
Published: May 27, 2021

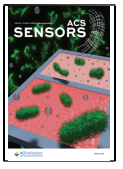

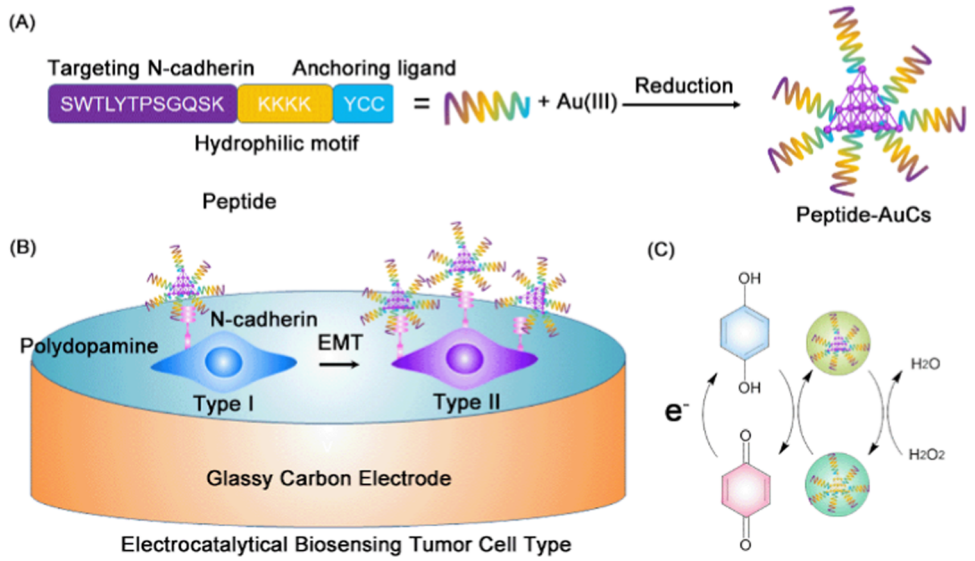

Figure 1. (A) Design of the peptide and precise synthesis of peptide-modified AuCs as the bioprobe. (B) Selective recognition of N-cadherin with AuCs and construction of the electrocatalytic biosensing system for detecting tumor cell biotypes during EMT using differential pulse voltammetry. (C) Proposed electrocatalytic mechanism of AuCs during detection.

nanomaterials with inherent surface heterogeneity, the potent electrochemical properties of metal clusters are suitable for the construction of a versatile modified electrode, in which the redox-active clusters serve as an electronic conductor and an electron-transfer mediator.[18] Recently, our group synthesized a series of metal cluster-based probes with definite molecular composition and optical property to analyze the distribution and abundance of the membrane proteins.[19] Considering that the enzyme-like properties of artificial nanoenzymes have been extensively investigated,[20−22] the enzyme-like properties of the metal clusters have been explored and used in the field of biomedical diagnosis and disease treatment.[23] Compared to other metal clusters with electrocatalytic properties, gold clusters (AuCs) are more suitable for the construction of an electrochemical sensing platform due to their better stability.[24] Here, we intend to extend the application of the well-designed AuCs to electrochemical sensing.

In this article, we develop a metal cluster-based electrochemical biosensing system to detect EMT progression by quantitatively analyzing N-cadherin in cancer cells. As shown in Figure 1A, an N-cadherin-targeting polypeptide sequence (SWTLYTPSGQSKKKKKYCC) is designed and peptide-protected AuCs are prepared by a moderate one-step biomimetic mineralization. To be specific, in this polypeptide with a domained function, SWTLYTPSGQSK targets and labels N-cadherin,[25] KKKK enhances the water solubility, and YCC reduces Au(III) to Au(0) and agglomerates Au(0) into metal clusters with the precise formulation. Further, polydopamine (PDA) is synthesized by chemical polymerization on the surface of a glassy carbon electrode (GCE) to fix tumor cells through an imine condensation reaction.[26] AuCs can be selectively captured by N-cadherin embedded in the surface of a tumor cell membrane owing to the targeting effect of polypeptides (Figure 1B).[27,28] Thus, EMT is evaluated by detecting the expression levels of the N-cadherin tumor biomarker through recording current signals from a AuC-catalyzed redox reaction between hydroquinone (HQ) and H_2O_2 (Figure 1C).[29,30] AuCs considerably accelerate the electron transfer and improve the sensitivity of the electrochemical biosensor. To our best knowledge, it is the first time to conduct antibody-free electrocatalytic analysis for absolutely quantifying membrane protein on intact tumor cells by metal clusters. On the basis of this system, we examined N-cadherin of cancer cells with different types. These findings are helpful to identify tumor cell-type transition. This electrochemical system holds great promise in analyzing cellular processes for early cancer diagnosis and monitoring.

EXPERIMENTAL SECTION

Materials and Apparatus. The peptide H_2N−SWTLYTPSGQSKKKKKYCC-COOH was synthesized by the standard solid-phase peptide synthesis technique (Beijing SciLight Biotechnology Ltd. Co., purity: 98%). Human pancreatic carcinoma PANC-1 and BxPC-3 cell lines were obtained from the Cell Resource Center, Institute of Basic Medicine, Chinese Academy of Medical Sciences. The Dulbecco's modified Eagle's medium (DMEM), glucose, and phosphate-buffered solution (PBS) were purchased from Hyclone (China). Fetal bovine serum (FBS) and trypsin−EDTA were acquired from Gibco. The human N-cadherin antibody and antirabbit IgG-HRP were purchased from Abcam Biotechnology (U.K.). Cell lysis buffer for western blotting, 4′,6-diamidino-2-phenylindole (DAPI) staining solution, and the bicinchoninic acid (BCA) protein assay kit were obtained from Beyotime Institute of Biotechnology (China). Matrigel, transwell plates were purchased from Corning Costar. Nitric acid (HNO_3), hydrochloric acid (HCl), sodium hydroxide (NaOH), HQ, and H_2O_2 were acquired from Beijing Chemical Reagent Co., China. Hydrogen tetrachloroaurate-(III) ($HAuCl_4{\cdot}4H_2O$) was purchased from Sinopharm Chemical Reagent Co., Ltd (China). Dopamine, $K_3Fe(CN)_6$, $K_4Fe(CN)_6$, copper sulfate ($CuSO_4$), and all components of buffer solutions were purchased from Sigma-Aldrich (Broendby, Denmark). Immobilon Western Chemiluminescent HRP Substrate was purchased from Millipore. Ultrapure water (18 MΩ) was used throughout the experiments. All of the reagents, chemicals, and solvents were of analytical grade and used without any further purification.

All electrochemical tests were performed in a conventional three-electrode cell on the Metrohm Autolab potentiostat/galvanostat system (PGSTAT302N, Switzerland) controlled with NOVA 2.1 software for data processing. The working, auxiliary, and reference electrodes were a glassy carbon electrode (GCE, 5 mm in diameter), a platinum plate electrode, and a KCl-saturated calomel electrode, respectively. The fluorescence spectra were characterized by a

https://doi.org/10.1021/acssensors.1c00339
ACS Sens. 2021, 6, 2290−2298

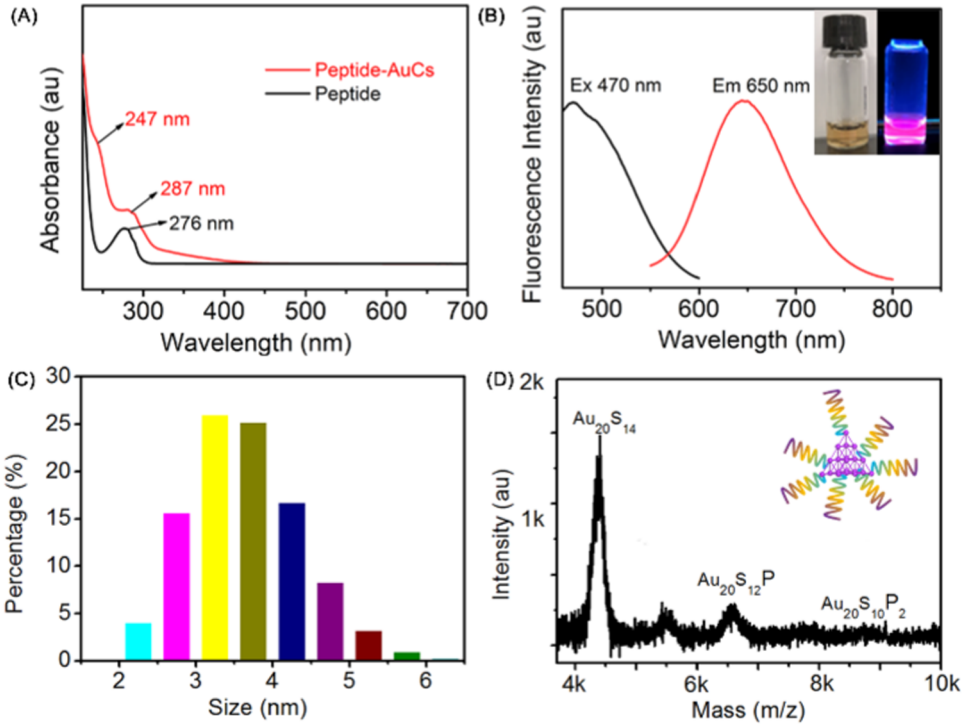

Figure 2. (A) UV−vis absorption spectra of the peptide and peptide-modified AuCs. (B) Fluorescence excitation and emission spectra of peptide-modified AuCs. Insets present images under sunlight and ultraviolet light. (C) Relevant DLS analysis and (D) MALDI-TOF MS measurement of AuCs.

spectrofluorometer (RF-5301, Shimadzu, Japan). UV−vis spectra were obtained by the UV-2600 spectrophotometer (Shimadzu, Japan). The hydrodynamic diameter of AuCs was measured at 25 °C, using a dynamic light scattering (DLS) particle sizer (Zetasizer Nano ZSE, Malvern, U.K.). To determine the accurate molecular formula of AuCs, AuCs were analyzed by matrix-assisted laser desorption/ionization time-of-flight mass spectrometry (MALDI-TOF MS) using an ABI MALDI-TOF system in a positive-ion linear mode. α-Cyano-4-hydroxycinnamic acid was used as the matrix. Surface morphological analysis of the tumor cells fixed on the working electrode was performed using S-4800 scanning electron microscopy (SEM, Hitachi, Japan). An ESCALAB 250Xi X-ray photoelectron spectroscope (XPS, Thermo Fisher, U.K.) and a VERTEX70 Fourier transform infrared spectroscope (FTIR, Bruker, Germany) were utilized to observe the change of electrode surface composition during the modification process. Bioprobe distribution on the cells was observed using a confocal laser scanning microscopy (CLSM) system (Nikon confocal fluorescence microscope and UltraVIEW VoX unit, Japan). JSY-SC-020H automatic cell counting instrument (China) was used for cell counting. The Tanon-5200 Chemiluminescence Multi Digital Image System (China) was used to detect the expression level of N-cadherin. The concentration of AuCs was analyzed using an inductively coupled plasma mass spectrometry (ICP-MS) analysis system (Thermo Elemental X7).

Synthesis of Peptide-Modified AuCs. Peptide-mineralized AuCs were synthesized according to the method previously proposed by our group. Briefly, all glassware were soaked in aqua regia before use and then rinsed with ultrapure water. A $HAuCl_4$ aqueous solution (25 mM, 180 μL) was dripped into a peptide solution (1.5 mM, 2980 μL) under vigorous shaking at 37 °C. Then, 0.5 mM NaOH was added to the mixture to adjust the pH to 12. The reaction continued for 24 h in the dark at 37 °C under continuous shaking to produce AuCs. Then, an ultrafiltration centrifuge tube (MWCO: 10 kDa) was utilized to purify the resultant clusters and remove the free peptides and ions. The purified samples were stored in darkness at 4 °C.

Specific Study of AuCs for N-Cadherin on PANC-1 and BxPC-3 Cells. Cell distribution study of AuCs on PANC-1 and BxPC-3 cells. PANC-1 and BxPC-3 cells were cultured on confocal dishes and incubated at 37 °C for 24 h. After being washed with PBS three times, the cells were fixed by 3.7% paraformaldehyde at room temperature for 15 min. Subsequently, 3% bovine serum albumin (BSA) was added to the cells to block the nonspecific recognition sites, and then the cells were incubated with 10 μM AuCs for 40 min at room temperature. Then, we washed the cells with PBS three times to remove the free AuCs. The cells in the blank control group were only treated with the medium. Next, the cells were stained with 5 μg mL^{-1} DAPI for 5 min and observed using a CLSM system.

Blocking Study. To further confirm the labeling specificity of AuCs, after being fixed with 3.7% paraformaldehyde and blocked with 3% BSA, the cells were incubated with a 5 mM free peptide for 1 h, followed by the addition of 10 μM AuCs for 40 min. Then, 5 μg mL^{-1} DAPI was introduced into the cells to stain the nuclei. After being thoroughly washed with PBS, the cells were imaged using a CLSM system.

Quantifying the Expression Level of N-Cadherin on PANC-1 and BxPC-3 Cells by ICP-MS. Rational cell-labeling efficiency was investigated by changing AuC concentration and incubation time. First, after being fixed by 3.7% paraformaldehyde, a series of AuCs with different concentrations (2.5, 5.0, 10, 15, 20 μM) were incubated with PANC-1 and BxPC-3 cells at room temperature for 40 min. We used PBS to wash samples three times and then counted the detached cells using automatic cell counting instrument. Subsequently, the cells labeled by AuCs were transferred to conical vials, and 4 mL of aqua regia was added to each conical vial. After 24 h, the cell samples were digested in a microwave reaction system. When evaporated to 0.1−0.2 mL, the sample was diluted with a mixed acid solution containing 2% HNO_3 and 1% HCl to a final volume of 5.0 mL. The Au standard calibration plot was obtained by injecting a series of Au standard solutions (0.1, 0.5, 1.0, 5.0, 10, 50 ng mL^{-1}). All samples were diluted to appropriate multiples and tested three times in parallel using the ICP-MS analysis system. For the time parameter, PANC-1 and BxPC-3 cells were incubated with a 10 μM AuC probe at different times (10, 20, 30, 40, 50 min) at room temperature. Other experimental steps

https://doi.org/10.1021/acssensors.1c00339
ACS Sens. 2021, 6, 2290−2298

were the same as those used to study the effect of AuC concentration on labeling efficiency.

Electrode Modification and Cell Immobilization. The surface of bare GCE was polished with 0.05 μm α-Al_2O_3 powder slurries until a mirror shiny surface appeared to remove oxide layers. Then, the electrode was sonicated in ultrapure water and ethanol before being dried by a nitrogen gas stream. The GCE electrode was immersed in a 50 mM pH 8.5 Tris buffer solution containing 2 mg mL^{-1} dopamine hydrochloride, 4 mM $CuSO_4$, and 20 mM H_2O_2 for 30 min, and then gently rinsed with ultrapure water to prepare PDA/GCE. After being completely air-dried, a series of 10 μL of AuCs with different concentrations were uniformly dropped and fixed onto the electrode surface and allowed to dry at room temperature to capture AuCs for preparing AuCs/PDA/GCE. The electrode was gently washed with doubly distilled water after every assembly process. After the differential pulse voltammetry (DPV) test, the series of AuCs/PDA complex on the electrode surface was scraped off as a whole for ICP-MS measurement to determine the amount of AuCs involved in the electrocatalytic reaction. For the experimental group, 10 μL of suspensions of different numbers of cells labeled by AuCs were fixed onto the electrode surface and dried at room temperature. To be specific, the cells in the culture dish were scraped off gently with a precooled cell scraper and collected in a centrifuge tube. After immobilizing cells with 3.7% paraformaldehyde and blocking the nonspecific sites with 3% BSA, the cells were incubated with 10 μM AuCs at room temperature for 40 min. Finally, the suspension of cells labeled by AuCs was obtained after the cells were washed with PBS three times. For in situ detection of N-cadherin, a series of different numbers of cells (0.50, 0.90, 1.2, 1.5, 2.0×10^4) labeled by AuCs were uniformly fixed onto the surface of the PDA/GCE electrode. The resulting cell-fixed electrode can be used for subsequent electrochemical tests.

RESULTS AND DISCUSSION

Synthesis and Characterization of Peptide-Modified AuCs. The peptide was synthesized by the standard solid-phase peptide synthesis technique. Peptide-modified AuCs were prepared according to the previous report.[31] Figure 2A suggests that the peptide solution shows an obvious absorption peak at 276 nm, which is attributed to tyrosine in the peptide sequence. Compared with the free peptide, peptide-modified AuCs present two other obvious absorption peaks at 247 and 287 nm, which result from the transformation of the tyrosine phenol group into a phenoxy structure oxidized by Au(III). In addition, the increase in the absorption value from 320 to 400 nm is assigned to the formation of AuCs. Furthermore, as shown in Figure 2B, peptide-modified AuCs exhibit maximum emission at 650 nm under a maximum excitation peak at 470 nm. As shown in the inset of Figure 2B, the yellowish AuC solution exhibits a bright red fluorescence under UV irradiation of 365 nm. As displayed in Figure 2C, dynamic light scattering (DLS) measurement was also performed to demonstrate that AuCs are well dispersed with an approximate diameter of 3.6 ± 0.4 nm. Since the cross-sectional diameter of N-cadherin is approximately 2.0−3.0 nm, it can be inferred that one N-cadherin can bind to one AuCs.[32] In addition, the exact atomic composition of peptide-modified AuCs was obtained using the MALDI-TOF MS technique. Figure 2D displays that there are several major peaks between 4k and 10k m/z. The most abundant peak was observed at 4388 m/z, which could be attributed to $Au_{20}S_{14}$. Since there are two cysteine residues in each peptide, it can be inferred that seven peptide chains should be wrapped around each Au_{20} core. Thus, the molecular formula of peptide-modified AuCs prepared is determined as $Au_{20}(peptide)_7$. Additionally, the concentration of AuCs can be determined by ICP-MS analysis for the following quantitative analysis (Supporting Information, eq 1). Moreover, the stability of peptide-modified AuCs was investigated by monitoring the fluorescence intensity at room temperature within 60 days (Figure S1). The result shows that it has no obvious change, indicating that these AuCs possess good stability and can be preserved for a long time to perform subsequent experiments.

Evaluation of N-cadherin Expression and Invasion Ability on EMT Model Cells. Pancreatic carcinoma, as a typical type of cancer associated with the EMT process, poses a great threat to human life due to its significantly increasing morbidity and fatality rates. Two pancreatic cancer cell lines, PANC-1 and BxPC-3 cells, were chosen as models because of the significant difference in the N-cadherin expression level and invasion ability.[33] We used western blotting to roughly detect the expression levels of N-cadherin (130 kDa) of PANC-1 and BxPC-3 cells, as shown in Figure 3A. The

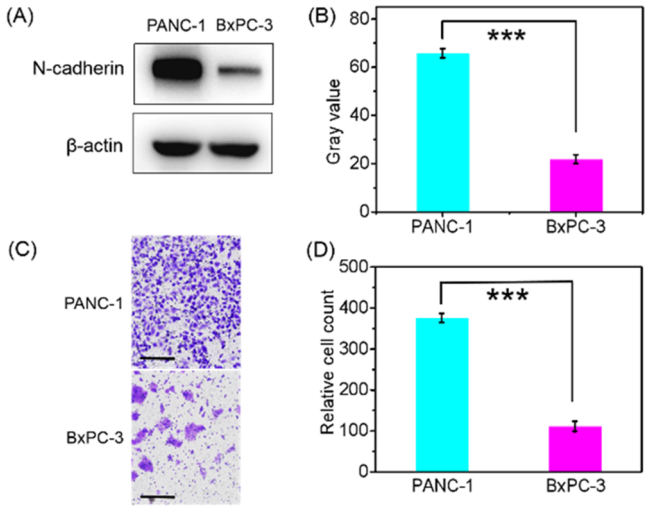

Figure 3. (A) Western immunoblotting semiquantitative analysis of N-cadherin in the total membrane protein extract after cells lysis. (B) Statistics of the gray value of the N-cadherin band. (C, D) Microscopy images and analysis of the invasion of PANC-1 and BxPC-3 cells. The scale bar represents 200 μm; ***$p < 0.001$.

corresponding statistics of the gray values (Figure 3B) reveal that the abundance of N-cadherin in PANC-1 cells is 2.0 times higher than that in BxPC-3 cells. Further, transwell assay was performed to verify the invasion ability of PANC-1 and BxPC-3 cells (Figure 3C). As shown in Figure 3D, PANC-1 cells exhibit 2.6 times higher longitudinal migration ability than BxPC-3 cells when passing through the transwell chamber. Taken together, these findings demonstrate that the N-cadherin expression level is positively related to the cells' invasion ability. Pancreatic cancer model cells were appropriately selected to study the biomarkers' variation during EMT, which ensures the reliability for evaluating the following electrochemical quantitative results.

Specific Recognition of Peptide-Modified AuCs. To verify the targeting ability of the AuC-based bioprobe, CLSM was employed to investigate whether AuCs could specifically recognize N-cadherin. As depicted in Figure 4A, after this bioprobe was coincubated with PANC-1 or BxPC-3 cells, the PANC-1 cells present a bright red fluorescence signal on the cytomembrane, while the BxPC-3 cells exhibit a relatively weaker fluorescence. The reason can be ascribed to the

https://doi.org/10.1021/acssensors.1c00339
ACS Sens. 2021, 6, 2290−2298

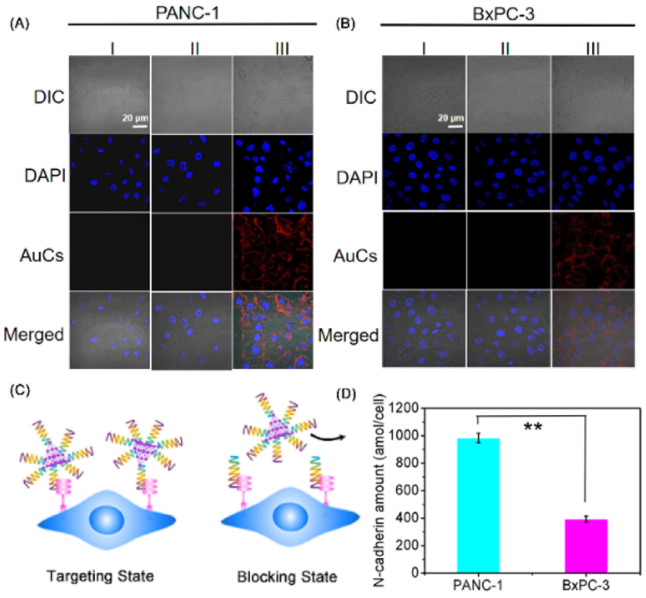

Figure 4. CLSM images of AuC-labeled (A) PANC-1 cells and (B) BxPC-3 cells. (I) control group, (II) blocking group, and (III) targeting group. (C) Relevant schematic diagram. (D) Quantitative analysis of N-cadherin in single PANC-1 and BxPC-3 cells by ICP-MS; $^{**}p < 0.01$.

different expression levels of N-cadherin in two cells. As a comparison, after free-peptide blocking, there is no obvious fluorescence on the PANC-1 or BxPC-3 cell membrane since the binding sites of N-cadherin are occupied by the free peptide (Figure 4C). This result confirms the specific recognition of the bioprobe to N-cadherin on the cell membrane.

Further, owing to the fact that AuCs have a concrete molecular formula and the recognition ratio of a single cluster to N-cadherin is 1:1, ICP-MS was employed to quantitatively detect the expression levels of N-cadherin on PANC-1 and BxPC-3 cell membranes. The optimal parameters, such as incubation time and AuC concentration, were determined before reliable quantitative detection. Figure S2A,B suggests that the content of Au labeled on the surface of a single cell increases along with increasing AuC concentrations. It reaches a plateau after the AuC concentration is up to 10 μM. Figure S2C,D shows that the average Au mass labeled on a single cell is no longer significantly increased after incubation for 40 min. Based on these results, the optimal AuC concentration is 10 μM and incubation time is 40 min. The following experiments were carried out under the optimal labeling conditions. Figure 4D reveals that after calculation, the amounts of the probe on single PANC-1 and BxPC-3 cells are 983 ± 34.1 and 392 ± 22.0 amol, respectively (Supporting Information, eq 2). After quantitative calculation (Supporting Information, eq 3), the expression numbers of N-cadherin in single PANC-1 and BxPC-3 cells were determined as $(5.92 \pm 0.21) \times 10^8$ and $(2.36 \pm 0.13) \times 10^8$, respectively. This finding is in agreement with the western blotting result above (Figure 3B), which further validates the specific recognition of peptide-modified AuCs.

Electrode Modification. To enhance the electrode performance and facilitate postfunctionalization, we engineered the surface of GCE via an oxidative polymerization reaction to form a PDA interface. Peptide-gold clusters were further fixed

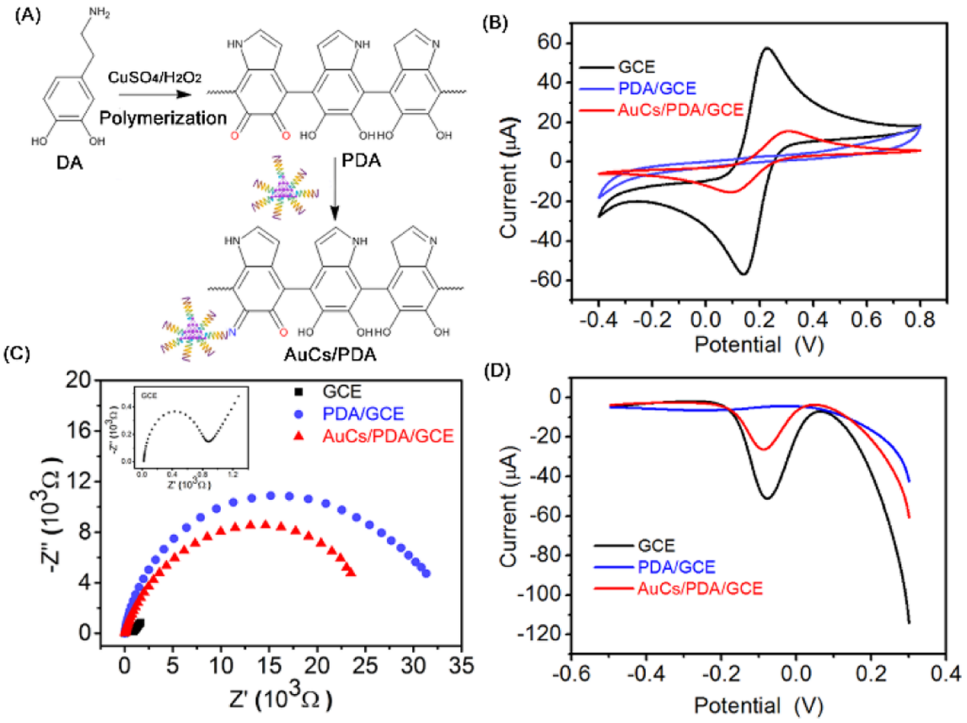

Figure 5. (A) Chemical modification of GCE with PDA and AuCs/ PDA. (B) Cycle voltammetry (CV) and (C) electrochemical impedance spectroscopy (EIS) spectra of bare GCE, PDA/GCE, and AuCs/PDA/GCE in 0.1 M pH 7.4 PBS containing 1.0 mM $K_3Fe(CN)_6$, 1.0 mM $K_4Fe(CN)_6$, and 0.2 M KCl. The inset of (C) represents the enlarged EIS spectrum of GCE. Note: the scan rate is 50 mV s^{-1} for CV, the frequency range is 100 kHz to 10 mHz, and amplitude is 5 mV for EIS. (D) DPV measurement of bare GCE, PDA/GCE, and AuCs/PDA/GCE in 0.1 M pH 7.4 PBS containing 10 mM HQ and 10 mM H_2O_2. Pulse amplitude is 25 mV and pulse width is 50 ms.

https://doi.org/10.1021/acssensors.1c00339
ACS Sens. 2021, 6, 2290−2298

through an imine condensation reaction between the terminal amino group of a peptide and a quinone moiety of PDA (Figure 5A). The optimal engineering conditions were determined according to the DPV peak current of the modified electrode. Figure S3 shows that the main factors have an effect on the DPV peak current of the modified electrode. After analysis, the optimal conditions are set as follows. The polymerization time is 30 min and the optimized concentrations of $CuSO_4$, HQ, and H_2O_2 are 4, 10, and 10 mM, respectively. In addition, we conducted experiments to investigate the influence of pH changes on the current signal (Figure S4). It shows that accompanying the increase in the pH value in the solution, the peak potential shifts negatively and the peak current increases and reaches a plateau when the pH value is 7.4. Thus, in our case, DPV tests were performed at pH 7.4, which is a typical physiological condition.

Furthermore, FTIR and XPS studies were employed to monitor electrode modification processes. As shown in Figure S5, the bending vibration peak of aromatic O−H and the symmetric vibration peak of C−O appear at 1340 and 1190 cm^{-1} in a dopamine monomer (black curve).[34] In contrast, after polymerization, in addition to the phenolic O−H stretching vibration peak at 1285 cm^{-1},[35] a strong absorption peak at 1550 cm^{-1} is considered as the characteristic peak of the indole structure of PDA.[36] Moreover, the peak at 1640 cm^{-1} is ascribed to C═O stretching vibrations in the quinones of PDA (red curve). As in the case of AuCs/PDA, a wide peak centered at 1600 cm^{-1} is assigned to C═N stretching vibrations, confirming the formation of Schiff-base covalent bonds between PDA and peptide-modified AuCs (blue curve).[37] Further, Figure S6 shows XPS spectra of the interface before and after modification of PDA and AuCs. After oxidative polymerization, the Cu element was successfully introduced. In addition, the Au element appears in the XPS pattern through modification of polydopamine by AuCs. Figure S7 shows the change in the surface morphology during the electrode modification process. In particular, for high-resolution XPS pattern of the deconvoluted C 1s, there is an obvious shift from 288.7 eV (pink curve in Figure S8A) to 288.0 eV (pink curve in Figure S8B), owing to the existence of C═N after conjugation.[38,39] As a whole, the abovementioned results indicate that the electrochemical biosensor AuCs/PDA/GCE is successfully constructed.

Besides, the effect of modification of electrode materials on charge-transfer behavior at the electrode/solution interface was investigated by cycle voltammetry (CV) and electrochemical impedance spectroscopy (EIS). CV curves in Figure 5B show the disappearance of redox peaks of $K_3Fe(CN)_6/K_4Fe(CN)_6$ after PDA deposition on the bare GCE due to poor electrical conductivity of PDA. Compared with PDA/GCE, the redox peak current of $K_3Fe(CN)_6/K_4Fe(CN)_6$ significantly increases on AuCs/PDA/GCE. Similarly, Nyquist impedance spectroscopy in Figure 5C reveals that electron-transfer resistance of AuCs/PDA/GCE is smaller than that of PDA/GCE, which is mainly attributed to the preferable electrochemical activity of AuCs. Furthermore, the electrocatalytic activity of the modified electrode materials toward HQ was performed by DPV. As shown in Figure 5D, a large reduction peak is observed on GCE around −0.08 V in pH 7.4 PBS containing 10 mM HQ and 10 mM H_2O_2, which disappears after PDA modification. AuCs have a good electrocatalytic activity because an obvious reduction peak appears on the AuCs/PDA/GCE as compared with PDA/GCE. These above-mentioned findings suggest that the good charge transfer and electrocatalytic activity of AuCs guarantee the successful preparation of the high-performance electrochemical sensor.

In Situ Electrochemical Detection of N-Cadherin. To implement the concept of utilizing the intrinsic electrocatalytic property of AuCs to quantify membrane protein expression, setting up a standard curve is the key point. The calibration plot of N-cadherin was profiled by the DPV method under optimal conditions after constructing the electrochemical biosensors containing peptide-modified AuCs (Figure 6A-I).

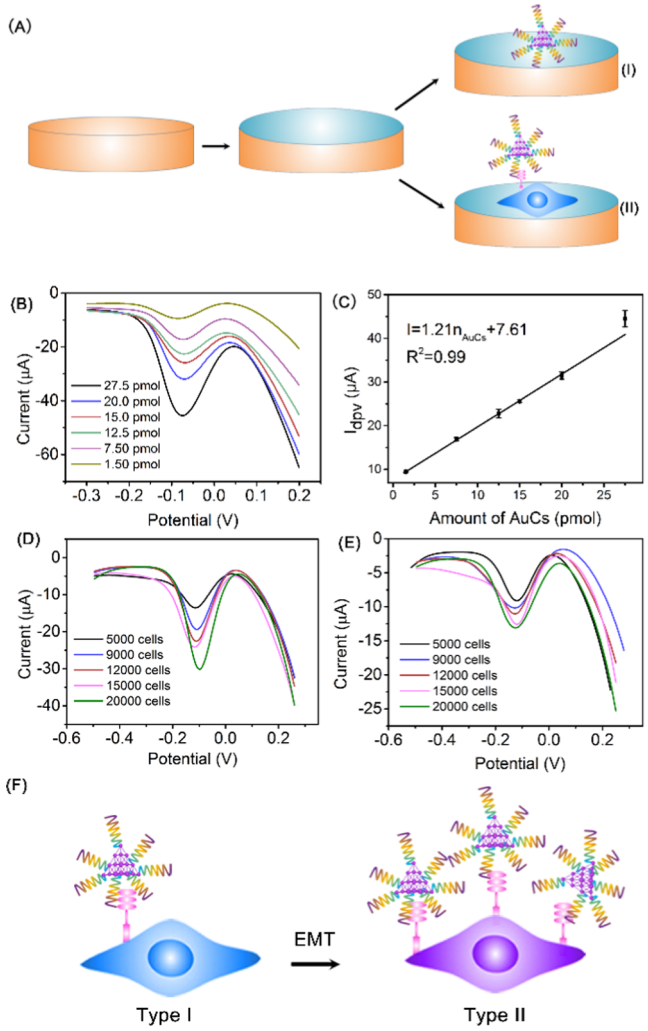

Figure 6. (A) Schematic illustration of the preparation of electrodes for detection of N-cadherin quantitatively. (B) DPV responses of AuCs/PDA/GCE to AuCs with different amounts fixed on the surface of PDA/GCE in 0.1 M pH 7.4 PBS containing 10 mM HQ and 10 mM H_2O_2. (C) Standard curve for this electrochemical analysis. Data are presented as mean ± standard deviation of triplicate experiments. DPV responses to (D) PANC-1 and (E) BxPC-3 cell numbers, respectively. (F) Schematic illustration of detection of EMT.

DPV peak current signals were first acquired according to the AuC-dependent electrocatalytic reaction. As shown in Figure 6B, the DPV peak current is increased with the enhanced amount of AuCs on the modified electrode surface. The plot of the DPV peak current value versus the amount of AuCs in Figure 6C is considered as the standard curve for this electrochemical analysis. It finds that there is an excellent linear relationship between the amount of AuCs and the DPV peak

https://doi.org/10.1021/acssensors.1c00339
ACS Sens. 2021, 6, 2290−2298

current signal. To be specific, in the range of 1.50−27.5 pmol of AuCs, the regression equation is $I = 1.21n_{AuCs} + 7.61$, with a high correlation coefficient of 0.99, where, I is the peak current of DPV curves and n_{AuCs} is the corresponding amount of AuCs.

To achieve in situ quantitative detection of N-cadherin, PANC-1 and BxPC-3 cells labeled with peptide-modified AuCs were immobilized on the surface of the PDA/GCE electrode (Figure 6A-II). To set control experiments, unlabeled cells with gradient numbers were modified onto the surface of PDA/GCE for DPV measurement and recorded as cells/PDA/GCE. As shown in Figure S9, there is no observable catalytic DPV current around −0.08 V. Therefore, the current signal is attributed to the intrinsic electrocatalytic property of AuCs. In other words, DPV current can reflect the content of AuCs. Figure 6D,E shows the DPV results of AuC-labeled tumor cells with different numbers (0.50, 0.90, 1.2, 1.5, 2.0 × 10^4) captured on the electrode surface. To confirm the stability of the cells trapped on the electrode surface, after DPV measurements, we observed cells' attachment on PDA/GCE by SEM. As shown in Figure S10, by comparing the cell counting results of the SEM images with those obtained from automatic cell counting instrument, it is found that the two counting results are almost the same, which ensures the accuracy of the cell count number on the electrode surface. In addition, the three-dimensional CLSM images in Figure S11 provide direct evidence of the monolayer distribution of tumor cells on the electrode surface. In detail, for PANC-1 cells, when the cell number varies from 0.50 × 10^4 to 2.0 × 10^4, the corresponding DPV peak current changes from 13.9 to 32.4 μA (Figure 6D). As a comparison, for BxPC-3 cells, it changes from 9.46 to 13.1 μA (Figure 6E). Based on the standard curve (Figure 6C), the amount of AuCs recognized on the cell membrane can be obtained. According to the precise molecular formula $Au_{20}(peptide)_7$ of this bioprobe, the number of N-cadherin on each cell can be calculated on the basis of the recognition ratio of one N-cadherin molecule per cluster. Taking 5000 cells as an example, the DPV peak current of the PANC-1 cell-modified electrode is 13.9 μA, while that of BxPC-3 is 9.46 μA. The corresponding amount of AuCs is 5.20 and 1.53 pmol, respectively. Therefore, the number of $Au_{20}(peptide)_7$ (equal to the amount of N-cadherin) recognized on each cell is 1049 ± 37.1 and 256.6 ± 34.1 amol (Supporting Information, eq 4), respectively. In other words, according to the calculation formula (Supporting Information, eq 5), the expression number of N-cadherin in each PANC-1 and BxPC-3 cell is about (6.32 ± 0.22) × 10^8 and (1.55 ± 0.21) × 10^8, respectively. These results are very close to those obtained from ICP-MS assay, which are (5.92 ± 0.21) ×10^8 and (2.36 ± 0.13) × 10^8, respectively. It further indicates that our strategy of in situ quantification of N-cadherin by the electrochemical method is reliable.

Further, to investigate whether our biosensor can be used to detect the tumor cells with lower N-cadherin, CaSki cells, a cervical cancer cell line, were selected (Text S7 and Figure S12). It shows that the expression level of N-cadherin in each CaSki cell is (8.20 ± 0.42) × 10^7, which is in good agreement with the result of ICP-MS, (7.93 ± 0.72) × 10^7. Based on the abovementioned findings, the linear range of our electrochemical analysis covers 7- to 8-fold of this biomarker expression, which can reflect the EMT process well in a certain range. Hence, this metal cluster-based electrochemical biosensing system can accurately and conveniently distinguish the different stages of EMT (Figure 6F). Since EMT plays crucial roles in cancer metastasis, multidrug resistance, stem cell initiation, and immunosuppression,[2,3] this rapid, precise, and reliable electrochemical system for quantifying the cellular expression of N-cadherin during EMT will assist in accessing the tumor progression efficiently.

CONCLUSIONS

In summary, the metal cluster-based bioprobe exhibits specific targeting and inherent electrocatalytic properties, which enables a precise, rapid, and reliable in situ electrochemical bioanalysis of oncobiomarkers without cell lysis. In particular, the active metal clusters function as both a redox mediator and an electronic conductor for quantitative electrochemical sensing. The expression level of N-cadherin on a single cell is calculated by coupling the precise molecular formula of a metal cluster with the recognition ratio of the metal cluster to protein. In addition, electrochemical quantification has excellent consistency with the results of mass spectrometry analysis. Hence, our metal cluster bioprobes provide the potent tool to detect expression levels of N-cadherin during EMT, which is highly related to the invasion and metastasis of cancer cells. This work gives important guidance for developing advanced probes for intact cell detection to differentiate the stages of diseases in clinics. In addition, since metal clusters produce the electrocatalytic current signals at disparate potentials, multiple biomarker detections can be achieved utilizing different metal cluster-based electrocatalysts after conjugation with recognizing peptides. We also envision that atomically modulated metal clusters will enable us to systematically optimize the electrochemical and surface properties suitable for electrocatalysis in the future.

ASSOCIATED CONTENT

Supporting Information

The Supporting Information is available free of charge at https://pubs.acs.org/doi/10.1021/acssensors.1c00339.

The formula of quantitative calculation, the stability of AuCs, optimization of conditions of cells labeled with AuCs, optimization of electrochemical test conditions, the influence of pH changes on the current signal, the characterization of the surface morphology and the structure of the modified electrode, the effect of pure cells on the current signal, and quantitative analysis of N-cadherin in CaSki cells with lower N-cadherin levels (PDF)

AUTHOR INFORMATION

Corresponding Author

Liang Gao − *Department of Chemistry and Biology, Faculty of Environment and Life Science, Beijing University of Technology, Beijing 100124, China;* orcid.org/0000-0002-9337-345X; Email: gaoliang@bjut.edu.cn

Authors

Ying Han − *Department of Chemistry and Biology, Faculty of Environment and Life Science, Beijing University of Technology, Beijing 100124, China*

Cuicui Qiu − *State Key Laboratory of Tribology, Tsinghua University, Beijing 100084, China*

Jiaojiao Li − *Department of Chemistry and Biology, Faculty of Environment and Life Science, Beijing University of Technology, Beijing 100124, China*

Fuping Gao − *CAS Key Laboratory for Biomedical Effects of Nanomaterials and Nanosafety, Institute of High Energy Physics, Chinese Academy of Sciences, Beijing 100049, China;* orcid.org/0000-0002-0287-9763

Qing Yuan − *Department of Chemistry and Biology, Faculty of Environment and Life Science, Beijing University of Technology, Beijing 100124, China;* orcid.org/0000-0003-4058-5931

Yuhua Tang − *Department of Chemistry and Biology, Faculty of Environment and Life Science, Beijing University of Technology, Beijing 100124, China*

Wenchao Niu − *Department of Chemistry and Biology, Faculty of Environment and Life Science, Beijing University of Technology, Beijing 100124, China*

Xiayan Wang − *Department of Chemistry and Biology, Faculty of Environment and Life Science, Beijing University of Technology, Beijing 100124, China;* orcid.org/0000-0003-1735-0077

Xueyun Gao − *Department of Chemistry and Biology, Faculty of Environment and Life Science, Beijing University of Technology, Beijing 100124, China;* orcid.org/0000-0002-2267-9945

Complete contact information is available at: https://pubs.acs.org/10.1021/acssensors.1c00339

Author Contributions

L.G. designed the research; Y.H., C.Q., J. L., F.G., Q.Y., Y.T., W.N., X.W., and X.G. performed the experiments; and Y.H. and L.G. analyzed data and wrote the paper. All authors have given approval to the final version of the manuscript.

Notes

The authors declare no competing financial interest.

■ ACKNOWLEDGMENTS

This work was financially supported by the Natural Science Foundation of China (31771082, 51705285, 21727817, U2067214, 11621505, 31971269, 31700874). The authors also acknowledge the financial support from the Beijing Municipal High Level Innovative Team Building Program (IDHT20180504), the Beijing Municipal Natural Science Foundation (KZ202010005005), the Beijing Outstanding Young Scientist Program (BJJWZYJH01201910005017), and the "Talented People Project" from Beijing University of Technology.

■ REFERENCES

(1) Wu, L.; Qu, X. Cancer biomarker detection: recent achievements and challenges. *Chem. Soc. Rev.* **2015**, *44*, 2963−2997.

(2) Thiery, J. P.; Acloque, H.; Huang, R. Y.; Nieto, M. A. Epithelial-mesenchymal transitions in development and disease. *Cell* **2009**, *139*, 871−890.

(3) Dongre, A.; Weinberg, R. A. New insights into the mechanisms of epithelial-mesenchymal transition and implications for cancer. *Nat. Rev. Mol. Cell Biol.* **2019**, *20*, 69−84.

(4) Du, X.; Zhang, Z.; Zheng, X.; Zhang, H.; Dong, D.; Zhang, Z.; Liu, M.; Zhou, J. An electrochemical biosensor for the detection of epithelial-mesenchymal transition. *Nat. Commun.* **2020**, *11*, No. 192.

(5) Padmanaban, V.; Krol, I.; Suhail, Y.; Szczerba, B. M.; Aceto, N.; Bader, J. S.; Ewald, A. J. E-cadherin is required for metastasis in multiple models of breast cancer. *Nature* **2019**, *573*, 439−444.

(6) Cao, Z. Q.; Wang, Z.; Leng, P. Aberrant N-cadherin expression in cancer. *Biomed. Pharmacother.* **2019**, *118*, No. 109320.

(7) Alberti, D.; van't Erve, M.; Stefania, R.; Ruggiero, M. R.; Tapparo, M.; Geninatti Crich, S.; Aime, S. A Quantitative Relaxometric Version of the ELISA Test for the Measurement of Cell Surface Biomarkers. *Angew. Chem.* **2014**, *126*, 3556−3559.

(8) Lee, H.; Park, J. E.; Nam, J. M. Bio-barcode gel assay for microRNA. *Nat. Commun.* **2014**, *5*, No. 3367.

(9) Chu, B.; Qi, T.; Liao, J.; Peng, J.; Li, W.; Fu, S.; Luo, F.; Zhiyong, Q. Colorimetric detection of cancer biomarker based on pH induced color change. *Sens. Actuators, B* **2012**, *166−167*, 56−60.

(10) Yang, Y.; Xia, T.; Zhang, W.; Fang, X. Single-molecule fluorescence imaging of membrane-bound proteins for studies of cell signal transduction. *Chin. Sci. Bull.* **2011**, *56*, 1063−1067.

(11) Feng, J.; Zhang, X.; Huang, L.; Yao, H.; Yang, C.; Ma, X.; Zhang, S.; Zhang, X. Quantitation of Glucose-phosphate in Single Cells by Microwell-Based Nanoliter Droplet Microextraction and Mass Spectrometry. *Anal. Chem.* **2019**, *91*, 5613−5620.

(12) Arya, S. K.; Kongsuphol, P.; Mi, K. P. Off surface matrix based on-chip electrochemical biosensor platform for protein biomarker detection in undiluted serum. *Biosens. Bioelectron.* **2017**, *92*, 542−548.

(13) Guo, Y.; Tao, J.; Li, Y.; Feng, Y.; Ju, H.; Wang, Z.; Ding, L. Quantitative Localized Analysis Reveals Distinct Exosomal Protein-Specific Glycosignatures: Implications in Cancer Cell Subtyping, Exosome Biogenesis, and Function. *J. Am. Chem. Soc.* **2020**, *142*, 7404−7412.

(14) Dai, Y.; Xu, W.; Liu, C. C. Immunoglobulin G-Based Steric Hindrance Assay for Protein Detection. *ACS Sens.* **2020**, *5*, 140−146.

(15) Li, C.; Liu, X.; Zhang, Y.; Chen, Y.; Du, T.; Jiang, H.; Wang, X. A novel nonenzymatic biosensor for evaluation of oxidative stress based on nanocomposites of graphene blended with CuI. *Anal. Chim. Acta* **2016**, *933*, 66−74.

(16) Cheng, H.; Wang, X.; Wei, H. Ratiometric electrochemical sensor for effective and reliable detection of ascorbic acid in living brains. *Anal. Chem.* **2015**, *87*, 8889−8895.

(17) Gao, Q.; Xu, S.; Guo, C.; Chen, Y.; Wang, L. Embedding Nanocluster in MOF via Crystalline Ion-Triggered Growth Strategy for Improved Emission and Selective Sensing. *ACS Appl. Mater. Interfaces* **2018**, *10*, 16059−16065.

(18) Kwak, K.; Lee, D. Electrochemistry of Atomically Precise Metal Nanoclusters. *Acc. Chem. Res.* **2019**, *52*, 12−22.

(19) Zhang, X.; Liu, R.; Shu, Q.; Yuan, Q.; Xing, G.; Gao, X. Quantitative Analysis of Multiple Proteins of Different Invasive Tumor Cell Lines at the Same Single-Cell Level. *Small* **2018**, *14*, No. 1703684.

(20) Cheng, H.; Zhang, L.; He, J.; Guo, W.; Zhou, Z.; Zhang, X.; Nie, S.; Wei, H. Integrated Nanozymes with Nanoscale Proximity for in Vivo Neurochemical Monitoring in Living Brains. *Anal. Chem.* **2016**, *88*, 5489−5497.

(21) Hu, Y.; Cheng, H.; Zhao, X.; Wu, J.; Muhammad, F.; Lin, S.; He, J.; Zhou, L.; Zhang, C.; Deng, Y.; Wang, P.; Zhou, Z.; Nie, S.; Wei, H. Surface-Enhanced Raman Scattering Active Gold Nanoparticles with Enzyme-Mimicking Activities for Measuring Glucose and Lactate in Living Tissues. *ACS Nano* **2017**, *11*, 5558−5566.

(22) Wang, X.; Qin, L.; Zhou, M.; Lou, Z.; Wei, H. Nanozyme Sensor Arrays for Detecting Versatile Analytes from Small Molecules to Proteins and Cells. *Anal. Chem.* **2018**, *90*, 11696−11702.

(23) Gao, L.; Zhang, Y.; Zhao, L.; Niu, W.; Gao, X.; et al. An artificial metalloenzyme for catalytic cancer-specific DNA cleavage and operando imaging. *Sci. Adv.* **2020**, *6*, No. eabb1421.

(24) Sun, Y.; Cai, X.; Hu, W.; Liu, X.; Zhu, Y. Electrocatalytic and photocatalytic applications of atomically precise gold-based nanoclusters. *Sci. China Chem.* **2020**, *63*, 1−11.

(25) Devemy, E.; Blaschuk, O. W. Identification of a novel N-cadherin antagonist. *Peptides* **2008**, *29*, 1853−1861.

(26) Zhang, C.; Ou, Y.; Lei, W. X.; Wan, L. S.; Ji, J.; Xu, Z. K. $CuSO_4/H_2O_2$-Induced Rapid Deposition of Polydopamine Coatings with High Uniformity and Enhanced Stability. *Angew. Chem., Int. Ed.* **2016**, *55*, 3054−3057.

(27) Mrówczyński, R.; Markiewicz, R.; Liebscher, J. Chemistry of polydopamine analogues. *Polym. Int.* **2016**, *65*, 1288−1299.

(28) Feng, T.; Ji, W.; Zhang, Y.; Wu, F.; Tang, Q.; Wei, H.; Mao, L.; Zhang, M. Zwitterionic Polydopamine Engineered Interface for In

Vivo Sensing with High Biocompatibility. *Angew. Chem., Int. Ed.* **2020**, *59*, 23445−23449.
(29) Tao, Y.; Lin, Y.; Ren, J.; Qu, X. A dual fluorometric and colorimetric sensor for dopamine based on BSA-stabilized Au nanoclusters. *Biosens. Bioelectron.* **2013**, *42*, 41−46.
(30) Yin, H.; Zhou, Y.; Xu, Z.; Wang, M.; Ai, S. Ultrasensitive electrochemical immunoassay for DNA methyltransferase activity and inhibitor screening based on methyl binding domain protein of MeCP2 and enzymatic signal amplification. *Biosens. Bioelectron.* **2013**, *49*, 39−45.
(31) Zhai, J.; Jia, Y.; Zhao, L.; Yuan, Q.; Gao, F.; Zhang, X.; Cai, P.; Gao, L.; Guo, J.; Yi, S.; Chai, Z.; Zhao, Y.; Gao, X. Turning On/Off the Anti-Tumor Effect of the Au Cluster via Atomically Controlling Its Molecular Size. *ACS Nano* **2018**, *12*, 4378−4386.
(32) Harrison, O. J.; Jin, X.; Hong, S.; Bahna, F.; Ahlsen, G.; Brasch, J.; Wu, Y.; Vendome, J.; Felsovalyi, K.; Hampton, C. M.; Troyanovsky, R. B.; Ben-Shaul, A.; Frank, J.; Troyanovsky, S. M.; Shapiro, L.; Honig, B. The extracellular architecture of adherens junctions revealed by crystal structures of type I cadherins. *Structure* **2011**, *19*, 244−256.
(33) Nakajima, S.; Doi, R.; Toyoda, E.; Tsuji, S.; Wada, M.; Koizumi, M.; Tulachan, S. S.; Ito, D.; Kami, K.; Mori, T. N-Cadherin Expression and Epithelial-Mesenchymal Transition in Pancreatic Carcinoma. *Clin. Cancer Res.* **2004**, *10*, 4125−4133.
(34) Yu, F.; Chen, S.; Chen, Y.; Li, H.; Yang, L.; Chen, Y.; Yin, Y. Experimental and theoretical analysis of polymerization reaction process on the polydopamine membranes and its corrosion protection properties for 304 Stainless Steel. *J. Mol. Struct.* **2010**, *982*, 152−161.
(35) Li, Z.; Wu, C.; Zhao, K.; Peng, B.; Deng, Z. Polydopamine-assisted synthesis of raspberry-like nanocomposite particles for superhydrophobic and superolelophilic surfaces. *Colloids Surf., A* **2015**, *470*, 80−91.
(36) Singer, F.; Schlesak, M.; Mebert, C.; Hohn, S.; Virtanen, S. Corrosion Properties of Polydopamine Coatings Formed in One-Step Immersion Process on Magnesium. *ACS Appl. Mater. Interfaces* **2015**, *7*, 26758−26766.
(37) Gao, L.; Fei, J.; Zhao, J.; Cui, W.; Cui, Y.; Li, J. pH- and redox-responsive polysaccharide-based microcapsules with autofluorescence for biomedical applications. *Chem. - Eur. J.* **2012**, *18*, 3185−3192.
(38) Fan, X.; Zhang, L.; Wang, M.; Huang, W.; Zhou, Y.; Li, M.; Cheng, R.; Shi, J. Constructing carbon-nitride-based copolymers via Schiff base chemistry for visible-light photocatalytic hydrogen evolution. *Appl. Catal., B* **2016**, *182*, 68−73.
(39) Gao, L.; Liu, M.; Ma, G.; Wang, Y.; Zhao, L.; Yuan, Q.; Gao, F.; Liu, R.; Zhai, J.; Chai, Z.; Zhao, Y.; Gao, X. Peptide-Conjugated Gold Nanoprobe: Intrinsic Nanozyme-Linked Immunsorbant Assay of Integrin Expression Level on Cell Membrane. *ACS Nano* **2015**, *9*, 10979−10990.

https://doi.org/10.1021/acssensors.1c00339
ACS Sens. 2021, 6, 2290−2298